HAL
open science

(BEDT-TTF)2Cu2(CN)3 Spin Liquid: Beyond the Average Structure

Pascale Foury-Leylekian, Vita Ilakovac-Casses, Victor Balédent, Pierre Fertey, Alla Arakcheeva, Ognjen Milat, Denis Petermann, Gilles Guillier, Kazuya Miyagawa, Kazushi Kanoda, et al.

To cite this version:

Pascale Foury-Leylekian, Vita Ilakovac-Casses, Victor Balédent, Pierre Fertey, Alla Arakcheeva, et al.. (BEDT-TTF)2Cu2(CN)3 Spin Liquid: Beyond the Average Structure. Crystals, 2018, 8 (4), pp.158. ⟨10.3390/cryst8040158⟩. ⟨hal-01830162⟩

HAL Id: hal-01830162

https://hal.sorbonne-universite.fr/hal-01830162v1

Submitted on 4 Jul 2018

HAL is a multi-disciplinary open access archive for the deposit and dissemination of scientific research documents, whether they are published or not. The documents may come from teaching and research institutions in France or abroad, or from public or private research centers.

L'archive ouverte pluridisciplinaire **HAL**, est destinée au dépôt et à la diffusion de documents scientifiques de niveau recherche, publiés ou non, émanant des établissements d'enseignement et de recherche français ou étrangers, des laboratoires publics ou privés.

Distributed under a Creative Commons CC BY 4.0 - Attribution - International License

crystals

MDPI

Article

$(BEDT\text{-}TTF)_2Cu_2(CN)_3$ Spin Liquid: Beyond the Average Structure

Pascale Foury-Leylekian [1,*], Vita Ilakovac-Casses [2,3], Victor Balédent [1], Pierre Fertey [4], Alla Arakcheeva [5], Ognjen Milat [6], Denis Petermann [1], Gilles Guillier [1], Kazuya Miyagawa [7], Kazushi Kanoda [7], Pere Alemany [8], Enric Canadell [9], Silvia Tomic [6] and Jean-Paul Pouget [1]

1 Laboratory of Solid State Physics, CNRS UMR 8502, Univ. Paris Sud, Paris Saclay University, 91405 Orsay CEDEX, France; victor.baledent@u-psud.fr (V.B.); denis.petermann@u-psud.fr (D.P.); guillier@lps.u-psud.fr (G.G.); pouget@lps.u-psud.fr (J.-P.P.)
2 UPMC, LCP-MR, Sorbonne University, CNRS UMR 7614, F-75252 Paris, France; vita.ilakovac-casses@upmc.fr
3 Department of Physcs, Cergy-Pontoise University, F-95031 Cergy-Pontoise, France
4 Synchrotron SOLEIL, L'Orme des Merisiers, Saint-Aubin, B.P. 48, F-91192 Gif-sur-Yvette, France; pierre.fertey@synchrotron-soleil.fr
5 Laboratory of Condensed Matter, EPFL, CH-1015 Lausanne, Switzerland; allaarakcheeva@gmail.com
6 Institute of Physics, Bijenička Cesta 46, HR-10000 Zagreb, Croatia; milat@ifs.hr (O.M.); stomic@ifs.hr (S.T.)
7 Department of Applied Physics, University of Tokyo, Tokyo 113-8656, Japan; kazuya@ap.t.u-tokyo.ac.jp (K.M.); kanoda@ap.t.u-tokyo.ac.jp (K.K.)
8 Department of Materials Science and Chemical Physics and Institute of Theoretical and Computational Chemistry (IQTCUB), University of Barcelona, Martí i Franquès 1, 08028 Barcelona, Spain; p.alemany@ub.edu
9 Institute of Materials Science of Barcelona (ICMAB-CSIC), Campus de la UAB, 08193 Bellaterra, Spain; canadell@icmab.es
* Correspondence: pascale.foury@u-psud.fr; Tel.: +33-169-156-055

Received: 27 February 2018; Accepted: 30 March 2018; Published: 4 April 2018

Abstract: We present here the first accurate determination of the exact structure of κ-$(BEDT\text{-}TTF)_2Cu_2(CN)_3$. Not only did we show that the room temperature structure used over the last twenty years was incorrect, but we were also able to correctly and precisely determine it. The results of our work provide evidence that the structure presents a triclinic symmetry with two non-equivalent dimers in the unit cell, which implies a charge disproportionation between the dimers. However, structural refinement shows that the charge disproportionation is quite weak at room temperature.

Keywords: mott transition; molecular spin liquids; geometrical frustration; X-ray diffraction

1. Introduction

One of the richest subjects of study in condensed matter over the last 30 years concerns Mott insulators with strong magnetic interactions and antiferromagnetic ground state in whose proximity unconventional superconductivity can emerge. A more fascinating and fertile situation occurs when spin frustration comes into play [1]. In such a case, long-range magnetic order can be easily suppressed by quantum fluctuations, and a quantum spin liquid (QSL) ground state is expected [2]. The strong magnetic frustration is typically achieved for localized S = 1/2 spins antiferromagnetically (AFM) coupled on a perfect triangular lattice [3]. However, the experimental realization of such a system turned out to be rare, and few inorganic QSLs with a triangular network of spins have been discovered [4–7]. Recently, two families of layered (2D) organic salts—κ phases of the BEDT-TTF

donors, κ-(BEDT-TTF)$_2$X, and β phases of the Pd(dmit)$_2$ acceptor, β-Y[Pd(dmit)$_2$]$_2$—have been found to present a quasi-ideal triangular lattice of S = 1/2 spins [8,9]. Here, BEDT-TTF stands for bis-ethylene-dithio-tetrathiafulvalene, and dmit is dimercaptoisotrithione; X and Y are, respectively, anionic and cationic species. In κ-(BEDT-TTF)$_2$X salts built with two dimers of BEDTT-TTF and two anions X per unit cell, half an electron per BEDT-TTF is transferred on average to the anion layer, leaving one hole per BEDT-TTF dimer and thus one S = 1/2 spin. A 2D array of inter-dimer transfer integrals (t_0, t_0') connects the spins 1/2 in a quasi-isotropic triangular lattice with a ratio t_0/t_0', which is in the range 0.6–1.1 [10–12]. Of particular interest is the κ-(BEDT-TTF)$_2$Cu$_2$(CN)$_3$ compound (here after named κ-ET-Cu) in which the t_0/t_0' ratio and thus J/J′ is very close to 1 and therefore presents a case of a strong degree of frustration. This property, in the presence of a strong AFM interaction between spins where J~250 K, has been considered as a necessary ingredient for QSL [13,14]. Indeed, NMR [13] and heat capacity [15] measurements performed a decade ago have provided evidence of a spin-liquid ground state in κ-ET-Cu.

However, this salt is also a $\frac{1}{4}$ filled 2D electron gas with strong electron–electron interactions: the onsite Coulomb repulsion U is comparable to the bandwidth $U/W \approx 1.8$ [10,16]. It can thus stabilize various competing electronic phases [17], which might strongly impact the QSL. In particular, one expects bond order waves (BOWs) where holes are localized on intermolecular bonds competing with charge order (CO) states, where the charge occupancy of the molecules is modulated. Due to the strong dimerization of the donor layer, κ-ET-Cu has one hole with spin 1/2 localized per dimer (i.e., on the intra-dimer bond) and is thus generally regarded as a Mott–Hubbard localized system. In addition, the possible emergence of a (polar) CO state in κ-ET-Cu is an important issue that should not be neglected since ferroelectricity induced by an ordering of electric dipoles on the BEDT-TTF molecular dimers has been suggested to drive the spin-order in the Mott–Hubbard phase of κ-(BEDT-TTF)$_2$Cu(SCN)$_2$Cl [18]. The coupling of the electric dipoles with the spins could be a possible mechanism for the stabilization of QSL [19–24].

It is now established that κ-ET-Cu presents a very rich pressure–temperature phase diagram. At ambient pressure, this salt exhibits a thermodynamic phase transition around 6 K [25] with significant lattice [25] and sound velocity [26] anomalies. Interestingly, a recent resonant inelastic X-ray scattering study has been able to probe in the anion layer the vibration spectra of N atoms sizably coupled to the donors (see below) and to measure the electron–phonon coupling [27]. Under a low pressure of 0.4 GPa, the system becomes metallic and superconducting [28].

In κ-(BEDT-TTF)$_2$X compounds, which all exhibit such a subtle coupling between spin, charge, and lattice degrees of freedom, it is obvious that the detailed structure and its thermal evolution has a strong influence on the spin coupling and Mott behavior. Moreover, the crystallographic structure of κ-ET-Cu is not obvious because this salt contains various intrinsic disorders within the anionic layer as well as in the molecular stack. The room temperature structure of κ-ET-Cu has been intensively studied [29–33]. More recent studies of the thermal evolution of the structure have also been published [11,12,34].

In all of these previous works, the structure is refined in the monoclinic and centrosymmetric P2$_1$/c space group. The structure consists of (b,c) layers of strongly dimerized BEDT-TTF molecules, with each dimer oriented approximately perpendicularly to its nearest neighbors. The four molecules of the unit cell are equivalent by the symmetry elements of the space group. BEDT-TTF layers alternate along the a direction with Cu$_2$CN$_3$ anionic layers. The anionic layer is composed of CuCN polymeric-like chains running along the **b** axis. There are two chains per unit cell related by the inversion center. The chains are connected by C–N groups (hereafter labeled C2–N2 and C10–N10). In the P2$_1$/c space group, the C2–N2 groups are located at the inversion center. These groups are thus expected to be disordered either dynamically or statistically. Within the molecular layer, the ethylene groups (C$_2$H$_4$) of the BEDT-TTF molecules are, depending on the structural refinement, either ordered [29,31] or partially disordered [11,34] at 300 K. Disorder should be at the origin of the large anisotropic displacement parameters (ADP) mentioned in [33]. Disorder will be discussed in detail in the present study.

The aim of this work is to accurately re-investigate the structure of κ-ET-Cu. We show in particular that the long-accepted 300 K structure is incorrect. The observation from 300 K down to 3 K of Bragg reflections forbidden in the $P2_1/c$ space group shows that κ-ET-Cu adopts either the $P\bar{1}$ or P1 space groups. This new symmetry definitively proves the existence of the two unequal dimers per unit cell, which implies the existence of a charge disproportionation between these dimers in the entire temperature range. However, the structural refinement performed at room temperature shows that inter-dimer charge disproportionation is quite weak. Such charge disproportionation theoretically proposed in [19–24], but not detected by optical measurements [35], could help to understand the relaxor-like dielectric behavior [36,37] and may give a long-awaited experimental support for the suggested role of spin-dipolar coupling in the establishment of QSL. Additionally, charge disproportionation not fixed by the crystal symmetry can vary under external constraints such as temperature or pressure. For example, its enhancement under pressure may favor a transition from the localized Mott–Hubbard state at ambient pressure to a metallic state that exhibits superconductivity.

2. Materials and Methods

High-quality single crystals of κ-ET-Cu were synthesized by electro-crystallization following the process used in [29,37]. Crystals appear like very thin plate-like samples of less than 1 mm^3. Their surface corresponds to the (b,c) plane. We have performed preliminary X-ray diffraction measurements using a Cu Kα radiation laboratory source. For this diffraction study, we used a homemade three-circle diffractometer equipped with a pulse tube cryogenerator allowing measurements from room temperature down to 3 K. The full data collection has been performed on the synchrotron radiation facility SOLEIL at the CRISTAL beam line using a Newport four-circle diffractometer equipped with a Rigaku Oxford Diffraction Atlas CCD detector at a wavelength of 0.6724 Å. About 17,000 reflections were collected. Data were processed using the CrysAlis Pro suite [38], taking into account two components of the likely twinned crystal. The ab initio structure was solved using the charge flipping algorithm and then refined by full-matrix least squares, using Jana2006 software [39]. Note that the introduction of twins only weakly improved the refinement. The twinning ratio was found to be around 50%. The twinning (twofold axis along the c direction) relates domains where the two different dimers of the unit cell are interchanged. It can be a macro- or micro-twinning. However, the size of the twinned domains cannot be lower than a few microns because all Bragg reflections have an experimental resolution.

First-principles calculations were carried out using a density functional theory (DFT) approach [40,41], which was developed for efficient calculations in large systems and implemented in SIESTA code [42–44]. We used the generalized gradient approximation (GGA) to DFT and, in particular, the functional of Perdew, Burke, and Ernzerhof [45]. Only the valence electrons are considered in the calculation, with the core being replaced by norm-conserving scalar relativistic pseudopotentials [46] factorized in the Kleinman–Bylander form [47]. We have used a split-valence double-ζ basis set including polarization orbitals with an energy shift of 10 meV for all atoms [48]. The energy cutoff of the real space integration mesh was 350 Ry. The Brillouin zone was sampled using a grid of $(5 \times 20 \times 20)$ k-points [49]. The crystal structure at room temperature was used for the calculations.

3. Results

3.1. Evidence for a $P2_1/c$ Symmetry Breaking

In the $P2_1/c$ (P 1 2_1/c 1) space group, *h0l* Bragg reflections are forbidden whenever *l* is odd (c glide mirror extinctions), and the *0k0* ones are forbidden for odd *k* indices (2_1 helicoidal axis extinctions). Our structural measurements performed with both synchrotron and laboratory X-ray radiation have evidenced at 300 K, the presence of the two kinds of forbidden reflections. It is important to notice that these features were systematically observed for the 15 different crystals measured, except for 2 that were very small ($30 \times 30 \times 30$ μm^3). However, for these two crystals, the intensity of the

Bragg reflections was already not high enough for the detection of weak satellite reflections. It is also important to mention that, intrinsically, in any X-ray pattern, the number of *0k0* reflections with odd *k* values is small. In the case of κ-ET-Cu, we observed only *010* and *030*, forbidden by the 2_1 symmetry operation, but they were systematically present. Figure 1 displays the reciprocal lattice reconstruction of the (**a***, **c***) reciprocal plane at 300 K, and the most prominent forbidden reflections are indicated. Before going any further, we checked the possibilities of different experimental artifacts that could have been at the origin of these additional intensities. A wavelength harmonic contamination (λ/2) was totally excluded. A twinning effect cannot explain the presence of such forbidden reflections because no symmetry operation applied to the reciprocal space of one domain without forbidden reflections can lead to reflections observed at very low angles, such as the one indexed as a *010* reflection. The possibility of a multiple scattering effect was also ruled out due to the weakness of the scattering factors in organic compounds and the systematic character of the forbidden effects. Its presence thus cannot be associated with an experimental artifact and since they are observed in all sizeable single crystals measured, we can conclude that this symmetry breaking is an intrinsic structural property of κ-ET-Cu at 300 K.

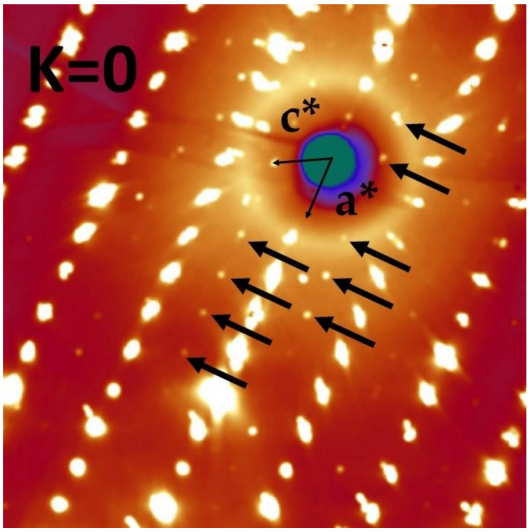

Figure 1. (Color online). Reconstruction of the (**a***, **c***) reciprocal plane taking into account the absorption correction. The thin arrows indicate the directions of the reciprocal lattice parameters, and the thick arrows show the reflections forbidden in the $P2_1/c$ space group.

In addition, all measured reflections, including the reflections forbidden in the $P2_1/c$ space group, had an experimental resolution. Furthermore, no particular diffuse scattering was detected. Finally, we observed not only low angle forbidden reflections but also high angle ones such as the *5013*. All of these features suggest that the presence of forbidden reflections does not originate from a thermal effect, nor from a disorder, but rather from an atomic displacement associated with a global symmetry breaking of the $P2_1/c$ structure. The average intensity of the forbidden reflections is 100 times lower than that of the main authorized Bragg reflections. The weakness of the intensity of the forbidden reflections indicates that the symmetry breaking is weak and explains that the previous structural studies have not detected this symmetry breaking with standard collect and refinement procedures.

Regarding the presence on the X-ray pattern of the various forbidden reflections, only the $P\bar{1}$ and P1 sub-groups of $P2_1/c$ are possible space groups for the real structure of κ-ET-Cu at 300 K. One can note that the triclinic angles α and γ are equal to 90° within error bars. The distinction between the P1 and $P\bar{1}$ space groups is very delicate from an experimental point of view. In particular, using X-rays, it is nearly impossible to differentiate both groups due to the Friedel law, which artificially creates a center of inversion in the X-ray pattern. We have then tried second harmonic generation measurements.

However, the transmission measurements at the usual wavelength of 1064 nm were not possible due to the fact that κ-ET-Cu is nearly metallic, being very close to the Mott insulator-to-metal transition boundary. Namely, no clear-cut optical gap has been observed, while the transport gap is less than 40 meV [16,37,50].

3.2. Structure at 300 K

For our refinements we used the $P\bar{1}$ space group as we could not detect the lack of inversion symmetry leading to P1.

3.2.1. Modeling of the Disorder

We used anisotropic displacement parameters (ADPs) for all the atomic species except for the hydrogen (H) atoms. Hydrogen atoms were placed at their ideal calculated positions and refined using a riding model. Each ethylene group of the BEDT-TTF molecule adopts a twist conformation as defined in Figure 2d. The two ethylene groups per BEDT-TTF molecule were however treated differently: the best structural model (i.e., the lowest R factors and the lowest electron density residuals) was obtained when the positions of the carbon atoms of one of the ethylene groups (the one on the left side of Figure 2a) were split over two symmetrically equivalent positions with respect to the plane of the molecule (e.g., Ci7–Ci7a and Ci8–Ci8a in Figure 2a), denoted as t and $\bar{t}$. The other ethylene group (the one on the right side of Figure 2a) was not split, and its configuration is t. The C–C distance of the symmetrically related ethylene groups as well as the carbon ADPs were kept identical. The fractional occupancy of each configuration was refined. This model led to staggered (S: t,t) (Figure 2b) and eclipsed (E: t,$\bar{t}$) Figure 2c bethylene conformations for each BEDT-TTF molecule, whose fractional occupancy reached 72% and 28% for the S and E conformations, respectively. These values agree with those obtained at 300 K in [29,34].

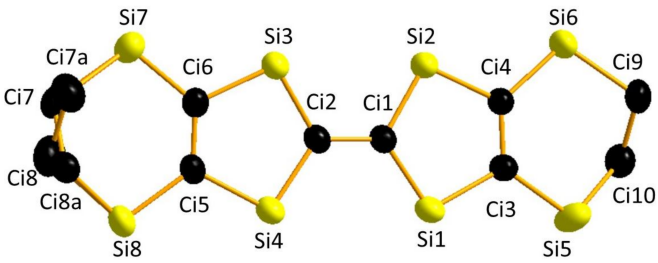

(**a**)

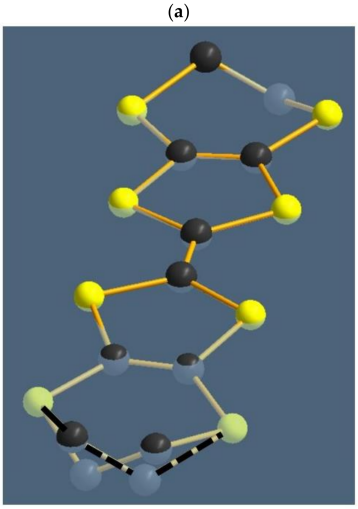

(**b**)

Figure 2. *Cont.*

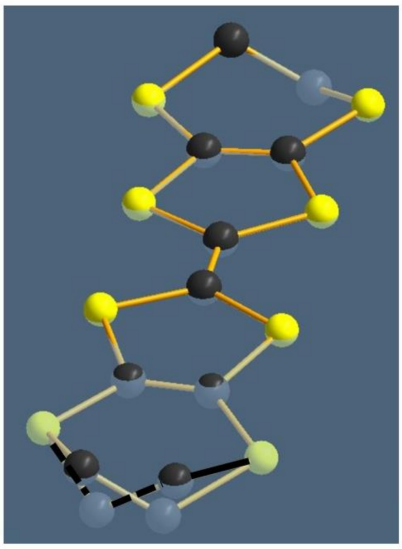

(**c**)

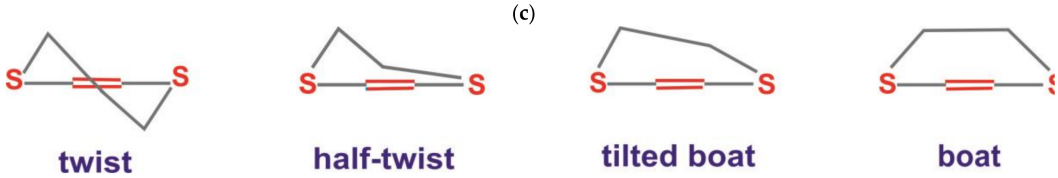

(**d**)

Figure 2. (Color online). (**a**) Ellipsoid of the ADPs at 300 K and labels for the various C and S atoms of the BEDT-TTF molecule i (i = 1 for Molecule 1 and i = 2 for Molecule 2). The two ethylene groups on the left side are in the t and $\bar{t}$ twist configurations (t and $\bar{t}$ are twist conformations symmetrically related with respect to the plane of the molecule). The ethylene group, which is not split, is also presented and is in the twist configuration. Schematic view of the terminal ethylene groups of the BEDT-TTF molecule in the (**b**) staggered (S: t, t) and (**c**) eclipsed (E: t,$\bar{t}$) conformations. The blue plane is the average molecular plane. Dashed lines represent part of the chemical bond below the average molecular plane; (**d**) Schematic representation of the four possible conformations of an ethylene group in the BEDT-TTF molecule (each ethylene group is represented by two C atoms and viewed along the long axis of the molecule). The energy of the conformation increases from left to right. Note that, in the twist conformation, there is a C atom on each side of the molecular plane and that, in the half-twist conformation, one C atom is in (or very near) the molecular plane. In the more energetic tilted-boat and boat conformations, the C atoms are on the same side of the molecular plane.

Within the anionic group, we have analyzed the disorder of the C2–N2 and C10–N10 groups located on the inversion center. We have first fitted the occupancy x of each site by an atom of carbon C (x) and an atom of nitrogen N (1-x). A total disorder corresponds to x = 0.5 and a total order to x = 0 or 1. However, as the X-ray scattering factors of C and N are nearly identical, we were not able to detect any reliable improvement of the refinement by varying x. We have thus decided to introduce an average scattering factor corresponding to 50% of C and 50% of N for each site of the disordered C–N groups.

3.2.2. Result of the Refinement

The best refinement of the structure at 300 K in the P$\bar{1}$ space group was obtained for the atomic positions and ADPs given in CCDC 1825317 (see details in [51]). The refinement led to R = 5.32%, wR = 8.35%, and N = 16338 reflections (14,479 with I > 2σ) for a total of 388 refined parameters, 184 constraints, and two restraints. The lattice parameters are a = 16.1221(10) Å, b = 8.591(6) Å, c = 13.412(8) Å, α = 89.99(2)°, β = 113.43(2)°, and γ = 90.01(2)°. The structure is shown in Figure 3a–c.

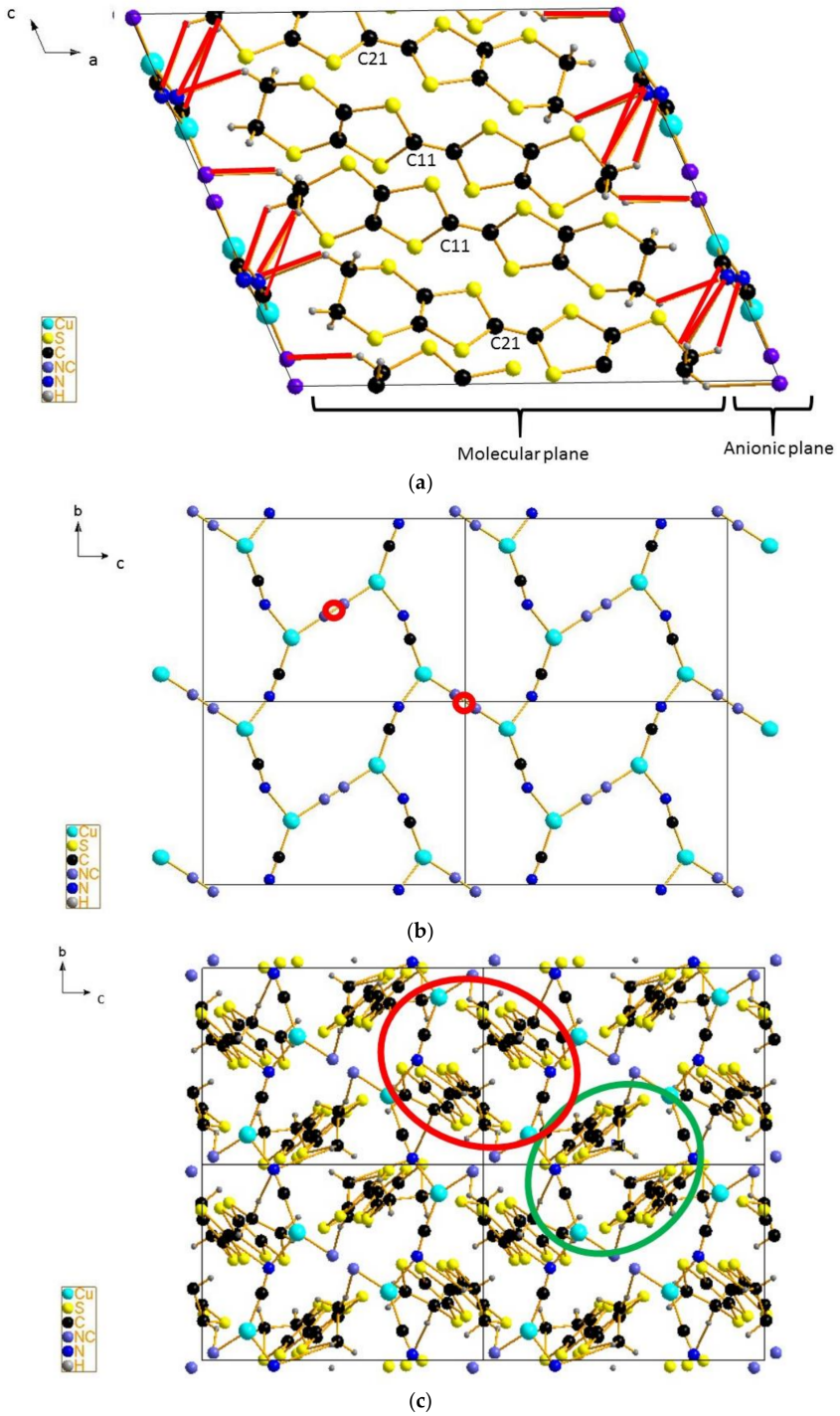

Figure 3. (**a**) (color online) Structure of κ-ET-Cu at 300 K viewed along the **b**-axis. For clarity purpose, only the most probable staggered C_2H_4 group configurations are represented. In the molecular layer, the first number of the atom labels (1 or 2) refers to the two different types of molecules and are indicated for the Ci1 atoms only. The hydrogen bonds (red lines) of the ethylene groups (S conformation) with the N and disordered N/C atoms in the anionic plane are also shown; (**b**) View of the anionic plane parallel to the (**b**,**c**) plane: the disordered C–N groups, which are located on the inversion centers (red circles), are colored in violet; (**c**) View of the anionic (**b**,**c**) plane and the molecular layer below showing Dimer 1 (green) and Dimer 2 (red).

The $P\bar{1}$ structure obtained is similar to the $P2_1/c$ ones previously published in [29–31] and more recently in [11,34]. In particular, the nearly flat shape of the core of the BEDT-TTF molecules is in agreement with the one expected theoretically and obtained in [11] and [31–33]. One can notice that, in the structure of [29], the molecules are more bent than in our structure and in the structures of [11] and [31–34]. In addition, typical distances of the Ci1–Ci2 double bonds (defined in Figure 2a and given in Table 1) of our structure are consistent with those expected for BEDT-TTF molecules with a +1/2 charge (half-hole) and those obtained in the refinements of [11] and [31–34], while in [29] these distances are significantly larger.

Table 1. Relevant interatomic distances for the structure at 300 K. The charge disproportionation 2δ defined in the text and calculated from the structural correlation as well as that from DFT calculations are also given.

Temperature	300 K
d_1(Å)	3.866(20)
d_2(Å)	3.872(20)
C1-C2 Dimer 1 (Å)	1.369(20)
C1-C2 Dimer 2 (Å)	1.372(20)
2δ (structural correlation) [52]	±0.06
2δ (DFT)	±0.01

Importantly, our density map indicates that, at room temperature, ethylene groups are slightly disordered. This is particularly the case of the Ci7–Ci8 groups (defined in Figure 2a), which are the closest ethylene groups to the disordered C–N groups. The ethylene groups of the BEDT-TTF molecules at 300 K are thus rather in a staggered twist conformation on each side of the molecule. The twist configuration presents the one of the lowest energy values for an isolated molecule [53,54] (see Figure 2d) as does that obtained by ab initio calculations in a similar compound [55]. This finding contrasts with the conclusion of refinements of [29,31] where an ordered configuration of the BEDT-TTF molecule was found at room temperature. These last refinements give a half-twist conformation of the ordered ethylene groups (see Figure 2d), which is not a conformation with the lowest energy. Note that a half-twist conformation was observed in BEDT-TTF molecules of salts exhibiting structural instabilities, such as α-(BEDT-TTF)$_2$I$_3$ and α-(BEDT-TTF)$_2$KHg(SCN)$_4$ salts [56]. The origin of the half-twist conformation of the ethylene groups in these salts seems to be due to the presence of constraints exerted by the environment of the BEDT-TTF molecules, i.e., the mechanical constraints due to the geometry of hydrogen bonds established with the anions.

Concerning the hydrogen bonds between the electropositive H atoms from the ethylene groups and the electronegative atoms of the anionic stack, their presence in organic systems is very frequent. It is an important structural effect that controls the packing of the BEDT-TTF layer and which is essential to stabilize various instabilities such as the CO ground state [57,58]. In the case of κ-ET-Cu, hydrogen bonds between the electropositive H atoms of the ethylene groups and the electronegative N or C atoms of the anionic stack are shown in Figure 3a. If one analyzes the hydrogen bond network between the BEDT-TTFs and the atoms of the anionic polymeric network shorter than 2.8 Å, it appears that the BEDT-TTFs of both dimers, when they are staggered, make two hydrogen bonds with N atoms (2.69 and 2.73 Å for Donor 1 and 2.68 and 2.75 Å for Donor 2) and another one with one of the atoms of the disordered CN group (2.74 Å for Donor 1 and 2.73 Å for Donor 2). When the donors are eclipsed they make two hydrogen bonds with N atoms (2.69 and 2.70 Å for Donor 1 and 2.69 and 2.68 Å for Donor 2) and another one with the C atoms (2.61 Å for Donor 1 and 2.55 Å for Donor 2). From these values, it is not clear if there is a net preference for the staggered conformation. The hydrogen bonds with the N atoms seem to slightly favor the eclipsed conformation. However, when both donors are staggered, they establish a short contact with the disordered CN group, whereas when they are

eclipsed they establish a short contact with the less electronegative C atom. It is most likely that the interaction with the anionic network does not clearly favor one of the two conformations.

In order to progress in the analysis of the origin of the disorder, one must also consider the interactions within the donor layers. Stabilizing S···H hydrogen bonds and H···H repulsive interactions have a strong influence on the actual conformation of the donors and hence on the occurrence of a disorder within the donor layers. When the donors are in the staggered or in the eclipsed conformations, there are no H···H contacts shorter than 2.40 Å (this would indicate repulsive interactions). Consequently, these contacts do not favor any of the two conformations. In contrast, the intra-dimer S···H hydrogen bonds favor an eclipsed conformation. In the eclipsed conformation, two intra-dimer S···H hydrogen bonds of 2.66 Å for Donor 1 and 2.60 Å for Donor 2 occur, but none of them is stabilized when the donors are in a staggered conformation. The inter-donor S···H interactions do not distinguish between the two conformations. Thus, as far as the inter-donor interactions within the BEDT-TTF layers are concerned, there is a preference for the eclipsed conformation.

Taking into account the previous analyses, we must conclude that the preference for a staggered conformation must originate from intra-BEDT-TTF interactions that must dominate over the inter-donor S···H interactions. In the absence of detailed first-principles calculations, it is not possible to clearly state whether or not the interaction with the anionic network favors one of the two conformations. What the present analysis suggests is that the preference for a staggered conformation originates from a competition between intra- and inter-donor interactions within the donor layers. Let us note that one reaches exactly the same conclusion when analyzing the $P2_1/c$ crystal structure of κ-ET-Cu at 300 K [11]. Thus, κ-ET-Cu is clearly different from other kappa salts of BEDT-TTF as, for instance, κ-(BEDT-TTF)$_2$Cu[N(CN)$_2$ X (X = Cl, Br). In these cases, a detailed structural analysis of the evolution of the crystal structure with temperature [56] clearly shows that the staggered minority conformation is favored by the interaction with the anionic network, whereas it is strongly disfavored by very short and repulsive H···H interactions within the BEDT-TTF dimer units. When the temperature is lowered, such repulsive interactions become too strong and all donors exhibit the eclipsed conformation. Clearly, the conformational preference of BEDT-TTF in kappa salts is a subtle question worth investigating.

3.3. Evolution of the Structure as a Function of Temperature

We have studied the thermal evolution of the structural properties of κ-ET-Cu as a function of temperature. Importantly, the $P\bar{1}$ space group is confirmed in the entire temperature range since reflections forbidden in the $P2_1/c$ space group were observed from 300 to 3 K. Upon cooling to 3 K, the intensity of these reflections only slightly increased, while the overall X-ray pattern did not change significantly. In particular, no significant change was detected in the temperature range between 300 and 200 K, where, according to H^1 NMR measurements [13], the thermally activated jump between E and S conformations decreases, leading to the stabilization of the S conformation seen in the structural refinements [11,34]. In addition, no substantial modification in the intensity of the Bragg reflections was observed in the temperature range between 60 and 3 K where a relaxor-like peak is detected by dielectric measurements [36,37].

Between κ-ET-Cu, on the one hand, and κ-(BEDT-TTF)$_2$Cu(SCN)$_2$ and κ-(BEDT-TTF)$_2$Cu[N(CN)$_2$]X where X = Br and Cl, on the other, the presence of different majority ethylene conformations (S versus E respectively) and the presence of a glass transition ascribed to the residual disorder between S and E ethylene configurations in the latter two salts, is quite noticeable.

Unfortunately, due to technical difficulties (the sample was not exactly on the axis of rotation) and to intrinsic problems related to the deconvolution of the two domains associated with the twin, which became impossible at low temperatures, we were not able to refine the low-temperature structures.

4. Discussion

4.1. Inter-Dimer Charge Disproportionation

The observation of a symmetry breaking from the previously accepted $P2_1/c$ space group to $P\bar{1}$ (or P1) has important implications. Within the $P2_1/c$ space group and consequently in the structures of references [11,29,31], the two BEDT-TTF molecules of a dimer are related by a center of inversion, and the two dimers of the unit cell are also related by symmetry. On the other hand, in the $P\bar{1}$ space group, the former symmetry is preserved, while the latter is broken. This should lead to differences between Dimer 1 and Dimer 2 in the present $P\bar{1}$ structure. First, their intra-dimer distance defined by the distance d between the core carbons of the two different molecules of a given dimer (all but the C atoms of the ethylene groups) should be different. Second, the slight deformation from the ideal BEDT-TTF molecular shape should also be different between the two dimers. This is, for instance, the case of the central Ci1–Ci2 bond length in Dimers 1 and 2. Indeed, Table 1 shows that these two types of distances are not identical, but their difference lies in the error bars.

The internal deformation of the molecules of a dimer can induce a charge deviation from the 0.5 holes per donor theoretically expected from the 2:1 stoichiometry (i.e., the BEDT-TTF charge is given as $0.5 \pm \delta$). We can extract the value of δ for a BEDT-TTF molecule from the relationship between internal structural parameters of the molecule and the associated charge given in [52]. The charges obtained at 300 K are +0.47 for a single BEDT-TTF in Dimer 1 and +0.53 for a single BEDT-TTF in Dimer 2, respectively (with a charge accuracy of 5% estimated from the bond length error bars). Note that this charge is not wholly determined by the central Ci1–Ci2 bond length, as is sometimes assumed. The normalized charge disproportionation thus obtained is $2\delta = 0.06 \pm 0.05$.

4.2. DFT Electronic Structure Calculation

To put these results on a firm basis, we have also carried out first-principles density functional theory (DFT) calculations. The temperature dependence of the electronic structure parameters assuming a $P2_1/c$ average structure was the subject of previous DFT studies [11,59]. Here, we are mostly interested in the magnitude of the charge difference between the two dimers. Because of the disorder of the C2–N2 and C10–N10 groups, we carried out two different types of calculation, using in both cases the crystal structure reported in this work. In the first calculation, the original $P\bar{1}$ structure has been converted into a P1 structure by selecting one of the two possible orientations of the CN pair at the inversion center but leaving the rest of the structure unaltered. In the second calculation, the anionic layer is completely removed from the calculation and the neutrality of the system is enforced using a uniform background of charge amounting to two electrons per unit cell. In that way, the $P\bar{1}$ original symmetry is kept. The density of holes per BEDT-TTF donor was calculated by integration of the density of states of the two upper HOMO bands and the two calculations led to the same charges. The calculated band structure for the 300 K structure is shown in Figure 4. The two upper bands are built from the anti-bonding combination of the two highest occupied molecular orbitals (HOMO) of the BEDT-TTF dimers. Figure 4 shows that these two bands nearly merge together along the Z–M and M–Y lines (there is degeneracy for the $P2_1/c$ space group). The separation between these two bands along the Z–M and M–Y lines is quite weak (between 3 and 5 meV). As this separation is proportional to the difference between the two types of dimers (i.e., the difference in energy of the HOMO's anti-bonding combination of each dimer and the difference in transfer integrals t_3 and t_4 between dimers of the same type along b), one obtains very similar intra- and inter-donor interactions for Dimers 1 and 2. This is confirmed by the fact that the DFT electronic structure dispersion of Figure 4 is nearly identical to the one of the $P2_1/c$ structure [11]. As expected from these results, despite the existence of the two different dimers, the holes are calculated to be practically equally shared by the two dimers ($2\delta \cong \pm 0.01$, which is of the same order of magnitude as the precision of our calculations). The results of vibrational spectroscopy [35], which do not reveal any charge imbalance larger than $\delta = \pm 0.01$e, agree with the present results despite the existence of two different dimers.

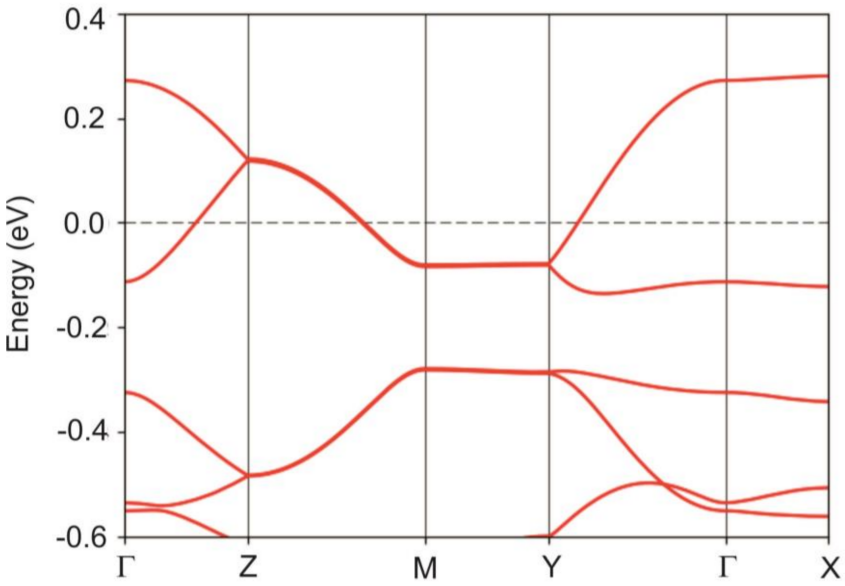

Figure 4. (Color online). Calculated band structure for the 300 K crystal structure of κ-ET-Cu. The energy zero corresponds to the Fermi level. Γ = (0,0,0), X = (1/2,0,0), Y = (0,1/2,0), Z = (0,0,1/2), and M = (0,1/2,1/2) in units of the reciprocal lattice vectors.

4.3. Inter-Dimer Charge Pattern

Figure 5a shows the BEDT-TTF pattern, which results from our structural refinements. The structure is made of rows of BEDT-TTF dimers of one type running along **b**. Rows of dimers of this type alternate with rows of dimers of the other type along **c**. The two types of dimers also alternate along the diagonal c ± b directions. Even if the charge disproportionation that results from the DFT calculations is small, it is permitted by symmetry of the new structure.

In order to further check the possibility of a sizeable charge disproportionation between dimers, we studied the hydrogen bond network between the anionic and donor layers. In previous studies of α-(BEDT-TTF)$_2$I$_3$ [58] and θ-(BEDT-TTF)$_2$MM′(SCN)$_4$ [60], it was shown that the hydrogen bond distance between the terminal C_2H_4 groups of BEDT-TTF and the anion reflects the degree of charge of the donor as a result of a subtle polarization mechanism detailed in [58]. Here, as discussed in detail above, the BEDT-TTF of Dimer 1 is related to the anionic plane by three short hydrogen bonds, smaller than 2.73 Å as well as the BEDT-TTF of Dimer 2, which is also connected by three hydrogen bonds shorter than 2.73 Å. This confirms that the charge of both dimers is practically equivalent, thus providing an indication of a weak charge disproportionation between dimers.

The charge disproportionation between dimers at room temperature, even weak, is real from a symmetry point of view. Thus, one should inquire as to the reasons for such a charge disproportionation in κ-ET-Cu as compared to other κ-(BEDT-TTF)$_2$X salts. One explanation could be that the charge disproportionation is due to the presence of stronger inter-site Coulomb repulsions. Such interactions are invoked to explain low-temperature CO ground states observed in several families of (BEDT-TT)$_2$X salts [17]. However, below the CO transition of such salts as well as of the Fabre salts, one observes an increase in the amplitude of the charge disproportionation upon cooling [61]. In the absence of low-temperature structural refinements allowing for the determination of the charge per donor, we cannot rule out this possibility. Another more likely possibility is that the charge disproportionation observed at room temperature is due to the presence of different environments of the BEDT-TTF dimers. The difference in environments is probably set by the anion sub-lattice and its H-bond interactions with the donors. Note that one of the hydrogen bonds for both types of dimers occurs with the disordered CN groups. Similar effects are observed in α-(BEDT-TTF)$_2$I$_3$ at room temperature and analyzed in [58].

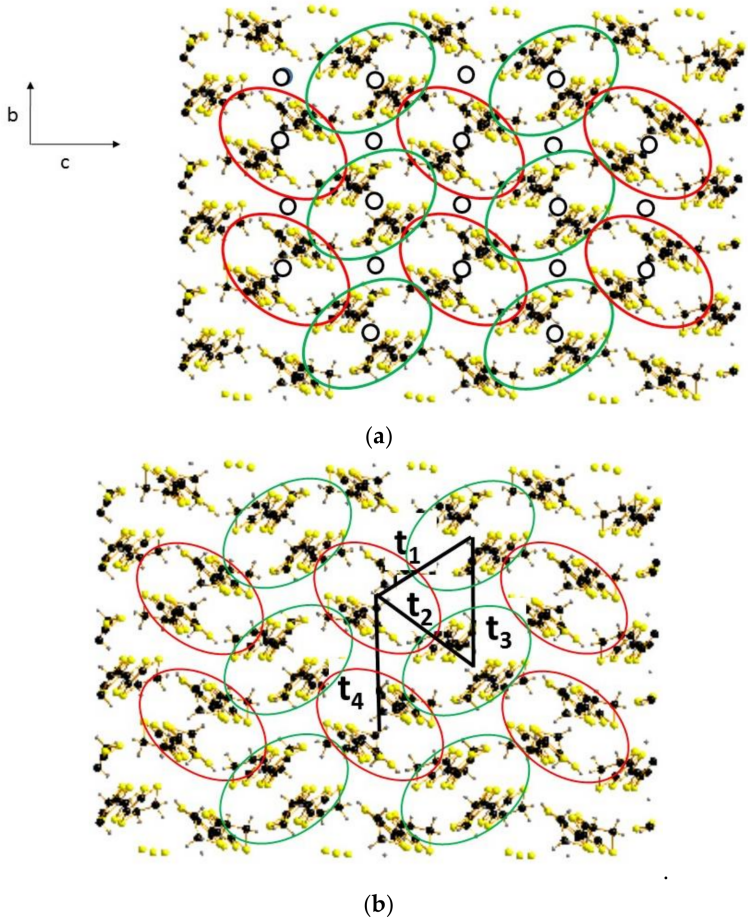

Figure 5. (Color online). (**a**) Molecular stack in the (**b**,**c**) plane showing the two types of dimers (red and green ellipses). The inversion centers remaining in the $P\bar{1}$ space group are indicated by black empty circles; (**b**) The same molecular stack with the four different transfer integrals (t_i with i = 1 to 4) between dimers represented by black segments.

Let us also remark that the finding of an intra-dimer distance that depends upon the charge of the dimer shows that the internal degrees of freedom of dimers that describe the physics of κ-ET-Cu cannot be ignored. This shows more generally that one must go beyond the simple dimer approximation where the electronic structure of κ-(BEDT-TTF)$_2$X is restricted to a simple set of t_i couplings (i = 1, 2, 3, and 4 in Figure 5b) between dimers.

Furthermore, it is important to realize that considering a prototype $P2_1/c$ structure containing two dimers per unit cell implies two possibilities to form charge-rich and charge-poor dimers in the $P\bar{1}$ structure. These two possibilities are achieved in different twinned domains whose ratio is estimated at 50% in our sample (see Section 4). Different twined domains where Dimers 1 and 2 are interchanged should be separated by polar domain walls where the position of charge-rich and charge-poor dimers interchanges. The motion of these domain walls should be at the origin of the observed dielectric response, whose relaxor-like nature also indicates the presence of disorder in κ-ET-Cu [37,59].

Although the detailed crystal structure analysis suggests that the main source of disorder may originate from the competition between intra- and inter-donor interactions in the donor layer, one must recall that one of the short hydrogen bonds between donor and the anion layers occurs with the disordered CN group of the anionic network. This CN disorder, which thus affects the whole (cation and anion) system, arises because of the triangular frustrated environment of Cu, where one bond links Cu with 50–50% CN (bridging CN), while two bonds link Cu to well-defined 100% CNs (CN chain). In the present refinement, we assume a complete orientation disorder of the bridging CN,

as the X-ray investigation is not able to give reliable information on this orientation disorder, as pointed above. Cu atoms are locally frustrated because they are coordinated either by two C atoms and one N atom or by one C atom and two N atoms. In that way, different anion–cation couplings/constrains are created, in particular via the establishment of N ... H bonds with the Ci7–Ci8 ethylene group (see Figure 2a). In the κ-ET-Cu structure, there is thus a robust zigzag chain motif with well-ordered CN chain groups along the ***b***-axis and different types of disordered C–N bridging groups (C2–N2 and C10–N10) along the ***c***-axis. Such a disorder may arise during the synthesis procedure where different C–N configurations can be obtained. As the charge redistribution among BEDT-TTF dimers may be altered by such disorder because the charge depends on the strength of the short donor-anion hydrogen bonds, the sample-dependent VRH and dielectric response can be explained [37,50].

4.4. Possible Intra-Dimer Charge Disproportionation

As detailed previously, our X-ray measurements are not able to discriminate between the P1 and the $P\bar{1}$ space groups. However, in the absence of an inversion symmetry (P1 space group), the molecules within a dimer are not equivalent. In that case, a charge disproportionation between the molecules of a dimer should exist and lead to weak electric dipoles. The intra-dimer electric dipoles have been assumed to theoretically explain the origin of the spin-liquid state via a dipolar-spin model based on a strong coupling analysis [19–21]. This scenario has been proposed earlier to interpret the relaxor-like dielectric properties of κ-ET-Cu [36] below 60 K. However, more recent results have shown that dipoles, if any, are weak and thus cannot be at the origin of the dielectric response [35,37,59].

4.5. Bringing Back Together the Puzzling Physical Behaviors

The presence of electric dipoles within the BEDT-TTF dimers has neither been detected by infrared [35] nor by terahertz [59,62] measurements. In particular, the ν_{27} peak has been investigated [35] because it is the most charge-sensitive infrared-active intra-molecular vibrational anti-symmetric mode related to the anti-symmetric ring Ci3–Ci4 and Ci5–Ci6 bonds of the BEDT-TTF molecules. No splitting of the mode has been detected within the error bars of 1 cm^{-1}, which corresponds to a charge disproportionation of 0.01e, thus giving evidence that no sizeable static charge intra-dimer disproportionation takes place.

Several models have been proposed to reconcile dielectric and optical measurements. The main model involves polar space groups: either $P2_1$ [37] or even P1 [59], which have been found energetically favorable by DFT calculations [59]. In the $P2_1$ space group, the C2–N2 and C10–N10 groups can be ordered because they are no more located on an inversion center. However, a geometrical frustration is present around a Cu atom bridging either 2N–1C or vice versa. This is expected to create domains and charge domain walls whose motion generates dielectric response. The latter scenario has also been investigated theoretically in [63]. Another model that assumes fluctuating intra/inter-dimer electric dipoles and that well explains the terahertz measurements of [62] has been developed. As argued in Section 3.3, the present structural investigation brings to light the presence of polar domain walls separating twin domains of the $P\bar{1}$ structure. Their motion could be the origin of the dielectric response.

Finally, it is important to note that preliminary X-ray scattering experiments on κ-ET-Ag [64] show that the same symmetry breaking from $P2_1/c$ to P1 or $P\bar{1}$ is present. This effect seems to be a general aspect of κ-(BEDT-TTF)$_2$M$_2$(CN)$_3$ (κ-ET-M), while no crystal lattice symmetry lowering in the orthorhombic phases of κ-(BEDT-TTF)$_2$Cu[N(CN)$_2$]X with X = Br [65–67] and Cl has been reported until now. It is important to observe that both κ-ET-Cu and κ-ET-Ag present a spin liquid state [68–70], which has not been observed in other κ-(BEDT-TTF)$_2$Cu[N(CN)$_2$] X compounds with X = Br and Cl. We can speculate that the structural particularities of κ-ET-M are a prerequisite to the emergence of the spin-liquid state.

An additional remark is that the charge disproportionation of κ-ET-Cu, which is not fixed by the crystal symmetry, can vary under external constraint such as temperature of pressure. For example if one assumes that with one hole per dimer (which value is confirmed within experimental

uncertainties by the present study) the insulating properties of κ-ET-Cu at ambient pressure arise from a Mott–Hubbard intra-dimer charge localization, the enhancement of inter-dimer charge disproportion under pressure should disfavor the localized state in favor of a metallic state, which presence is a necessary condition to stabilize superconductivity.

Acknowledgments: We thank Joon I. Jang for his work related to SHG measurements. S.T. acknowledges the support by the Croatian Science Foundation project IP-2013-11-1011. Work in Spain was supported by the Spanish Ministerio de Economía y Competitividad (Grants FIS2015-64886-C5-4-P and CTQ2015-64579-C3-3-P) and Generalitat de Catalunya (217SGR1506 and XRQTC). E.C. acknowledges the support of the Spanish MINECO through the Severo Ochoa Centers of Excellence Program under Grant SEV-2015-0496.

Author Contributions: Kazuya Miyagawa and Kazushi Kanoda were involved in the synthesis of the compound. Pascale Foury-Leylekian, Vita Ilakovac, and Pierre Fertey designed the synchrotron experiment. Victor Baledent and Ognjen Milat performed the first laboratory X-ray measurements. Pascale Foury-Leylekian, Alla Arakcheeva, Pierre Fertey, and Enric Canadell refined the data. Denis Petermann and Gilles Guillier made an important technical contribution to the laboratory measurements at low temperature. Pere Alemany performed the DFT calculations. Pascale Foury-Leylekian, Silvia Tomic, Enric Canadell, and Jean-Paul Pouget were involved in the physical analysis of the structural results and in the preparation of the manuscript. All authors contributed to and commented on the final manuscript.

Conflicts of Interest: The authors declare no conflict of interest.

References and Note

1. Powell, B.J.; McKenzie, R.H. Quantum frustration in organic Mott insulators: From spin liquids to unconventional superconductors. *Rep. Prog. Phys.* **2011**, *74*, 056501. [CrossRef]
2. Balents, L. Spin liquids in frustrated magnets. *Nature* **2010**, *464*, 199–208. [CrossRef] [PubMed]
3. Anderson, P.W. Resonating valence bonds: A new kind of insulator? *Mater. Res. Bull.* **1973**, *8*, 153–160. [CrossRef]
4. Coldea, R.; Tennant, D.A.; Tsvelik, A.M.; Tylczynski, Z. Experimental Realization of a 2D Fractional Quantum Spin Liquid. *Phys. Rev. Lett.* **2001**, *86*, 1335. [CrossRef] [PubMed]
5. Li, Y.; Liao, H.; Zhang, Z.; Li, S.; Jin, F.; Ling, L.; Zhang, L.; Zou, Y.; Pi, L.; Yang, Z.; et al. Gapless quantum spin liquid ground state in the two-dimensional spin-1/2 triangular antiferromagnet $YbMgGaO_4$. *Sci. Rep.* **2015**, *5*, 16419. [CrossRef] [PubMed]
6. Khuntia, P.; Kumar, R.; Mahajan, A.V.; Baenitz, M.; Furukawa, Y. Spin liquid state in the disordered triangular lattice $Sc_2Ga_2CuO_7$ revealed by NMR. *Phys. Rev. B* **2016**, *93*, 140408(R). [CrossRef]
7. Klanjšek, M.; Zorko, A.; Žitko, R.; Mravlje, J.; Jagličić, Z.; Biswas, P.; Prelovšek, P.; Mihailovic, D.; Arčon, D. A high-temperature quantum spin liquid with polaron spins. *Nat. Phys.* **2017**, *13*, 1130–1134. [CrossRef]
8. Kanoda, K.; Kato, R. Mott Physics in Organic Conductors with Triangular Lattices. *Annu. Rev. Condens. Matter Phys.* **2011**, *2*, 167–188. [CrossRef]
9. Zhou, Y.; Kanoda, K.; Ng, T.-K. Quantum spin liquid states. *Rev. Mod. Phys.* **2017**, *89*, 025003. [CrossRef]
10. Kandpal, H.C.; Opahle, I.; Zhang, Y.-Z.; Jeschke, H.O.; Valenti, R. Revision of Model Parameters for κ Type Charge Transfer Salts: An Ab Initio Study. *Phys. Rev. Lett.* **2009**, *103*, 067004. [CrossRef] [PubMed]
11. Jeschke, H.O.; de Souza, M.; Valenti, R.; Manna, R.S.; Lang, M.; Schlueter, J.A. Temperature dependence of structural and electronic properties of the spin-liquid candidate κ-$(BEDT\text{-}TTF)_2Cu_2(CN)_3$. *Phys. Rev. B* **2012**, *85*, 035125. [CrossRef]
12. Koretsune, T.; Hotta, C. Evaluating model parameters of the κ-and β′-type Mott insulating organic solids. *Phys. Rev. B* **2014**, *89*, 045102. [CrossRef]
13. Miyagawa, Y.S.K.; Kanoda, K.; Maesato, M.; Saito, G. Spin Liquid State in an Organic Mott Insulator with a Triangular Lattice. *Phys. Rev. Lett.* **2003**, *91*, 107001.
14. Zheng, W.; Singh, R.R.P.; McKenzie, R.H.; Coldea, R. Temperature dependence of the magnetic susceptibility for triangular-lattice antiferromagnets with spatially anisotropic exchange constants. *Phys. Rev. B* **2005**, *71*, 134422. [CrossRef]
15. Yamashita, S.; Nakazawa, Y.; Oguni, M.; Oshima, Y.; Jojiri, H.; Miyagawa, K.; Kanoda, K. Thermodynamic properties of a spin-1/2 spin-liquid state in a κ-type organic salt. *Nat. Phys.* **2008**, *4*, 459–462. [CrossRef]
16. Pustogow, A.; Bories, M.; Löhle, A.; Rösslhuber, R.; Zhukova, E.; Gorshunov, B.; Tomić, S.; Schlueter, J.A.; Hübner, R.; Hiramatsu, T.; et al. Quantum Spin Liquids Unveil the Genuine Mott State. *arXiv*, 2017.

17. Seo, H.; Merino, J.; Yoshioka, H.; Ogata, M. Theoretical Aspects of Charge Ordering in Molecular Conductors. *J. Phys. Soc. Jpn.* **2006**, *75*, 051009. [CrossRef]
18. Lunkenheimer, P.; Müller, J.; Krohns, S.; Schrettle, F.; Loidl, A.; Hartmann, B.; Rommel, R.; de Souza, M.; Hotta, C.; Schlueter, J.A.; et al. Multiferroicity in an organic charge-transfer salt: Electric-dipole-driven magnetism. *Nat. Mater.* **2012**, *11*, 755–758. [CrossRef] [PubMed]
19. Hotta, C. Theories on Frustrated Electrons in Two-Dimensional Organic Solids. *Crystals* **2012**, *2*, 1155–1200. [CrossRef]
20. Naka, M.; Ishihara, S. Electronic Ferroelectricity in a Dimer Mott Insulator. *J. Phys. Soc. Jpn.* **2010**, *79*, 063707. [CrossRef]
21. Li, H.; Clay, R.T.; Mazumdar, S. The paired-electron crystal in the two-dimensional frustrated quarter-filled band. *J. Phys. Condens. Matter* **2010**, *22*, 272201. [CrossRef] [PubMed]
22. Gomi, H.; Imai, T.; Takahashi, A.; Aihara, M. Purely electronic terahertz polarization in dimer Mott insulators. *Phys. Rev. B* **2010**, *82*, 035101. [CrossRef]
23. Gomi, H.; Ikenaga, M.; Hiragi, Y.; Segawa, D.; Takahashi, A.; Inagaki, T.J.; Aihara, M. Ferroelectric states induced by dimer lattice disorder in dimer Mott insulators. *Phys. Rev. B* **2013**, *87*, 195126. [CrossRef]
24. Gomi, H.; Inagaki, T.J.; Takahashi, A. A ferroelectric charge order enhanced by magnetic frustration in dimer Mott insulators. *Phys. Rev. B* **2016**, *93*, 035105. [CrossRef]
25. Manna, R.S.; de Souza, M.; Brűhl, A.; Schlueter, J.A.; Lang, M. Lattice Effects and Entropy Release at the Low-Temperature Phase Transition in the Spin-Liquid Candidate κ-(BEDT-TTF)$_2$Cu$_2$(CN)$_3$. *Phys. Rev. Lett.* **2010**, *104*, 016403. [CrossRef] [PubMed]
26. Poirier, M.; de Lafontaine, M.; Miyagawa, K.; Kanoda, K.; Shimizu, Y. Ultrasonic investigation of the transition at 6 *K* in the spin-liquid candidate κ-(BEDT-TTF)$_2$Cu$_2$(CN)$_3$. *Phys. Rev. B* **2014**, *89*, 045138. [CrossRef]
27. Ilakovac, V.; Carniato, S.; Foury-Leylekian, P.; Tomić, S.; Pouget, J.-P.; Lazić, P.; Joly, Y.; Miyagawa, K.; Kanoda, K.; Nicolaou, A. Resonant inelastic x-ray scattering probes the electron-phonon coupling in the spin liquid κ-(BEDT-TTF)$_2$Cu$_2$(CN)$_3$. *Phys. Rev. B* **2017**, *96*, 184303. [CrossRef]
28. Kurosaki, Y.; Shimizu, Y.; Miyagawa, K.; Kanoda, K.; Saito, G. Mott Transition from a Spin Liquid to a Fermi Liquid in the Spin-Frustrated Organic Conductor κ-(ET)$_2$Cu$_2$(CN)$_3$. *Phys. Rev. Lett.* **2005**, *95*, 177001. [CrossRef] [PubMed]
29. Geiser, U.; Wang, H.H.; Carlson, K.D.; Williams, J.M.; Charlier, H.A.; Heindl, J.E.; Yaconi, G.A.; Love, B.J.; Lathrop, M.W.; Schirber, J.E.; et al. Superconductivity at 2.8 K and 1.5 kbar in K-(BEDT-TTF)$_2$Cu$_2$(CN)$_3$: The first organic superconductor containing a polymeric copper cyanide anion. *Inorg. Chem.* **1991**, *30*, 2586–2588. [CrossRef]
30. Bu, X.; Frost-Jensen, A.; Allendoerfer, R.; Coppens, P.; Lederle, B.; Naughton, M.J. Structure and properties of a new κ-phase organic metal: (BEDT-TTF)$_2$Cu$_2$(CN)$_3$. *Solid State Commun.* **1991**, *79*, 1053–1057. [CrossRef]
31. Bu, X.; Coppens, P. Zeitschrift für Kristallographie. *New Cryst. Struct.* **1997**, *212*, 103–104.
32. Yamochi, H.; Nakamura, T.; Komatsu, T.; Matsukawa, N.; Inoue, T.; Saito, G. Crystal and electronic structures of the organic superconductors, $\varkappa$-(BEDT-TTF)$_2$Cu (CN)[N(CN)$_2$] and $\varkappa'$-(BEDT-TTF)$_2$Cu$_2$(CN)$_3$. *Solid State Commun.* **1992**, *82*, 101–105. [CrossRef]
33. Papavassiliou, G.C.; Lagouvardos, D.J.; Terzis, A.; Hountas, A.; Hilti, B.; Zambounis, J.S.; Mayer, C.W.; Pfeiffer, J.; Hofherr, W.; Delhaes, P.; et al. Physical properties in the normal state of the molecular superconductor κ-(BEDT)$_2$Cu$_2$(CN)$_3$. *Synth. Met.* **1993**, *61*, 267–273. [CrossRef]
34. Hiramatsu, T.; Yoshida, Y.; Saito, G.; Otsuka, A.; Yamochi, H.; Maesato, M.; Shimizu, Y.; Ito, H.; Kishida, H. Quantum spin liquid: Design of a quantum spin liquid next to a superconducting state based on a dimer-type ET Mott insulator. *J. Mater. Chem. C* **2015**, *3*, 1378–1388. [CrossRef]
35. Sedlmeier, K.; Elsässer, S.; Neubauer, D.; Beyer, R.; Wu, D.; Ivek, T.; Tomić, S.; Schlueter, J.A.; Dressel, M. Absence of charge order in the dimerized κ-phase BEDT-TTF salts. *Phys. Rev. B* **2012**, *86*, 245103. [CrossRef]
36. Abdel-Jawad, M.; Terasaki, I.; Sasaki, T.; Yoneyama, N.; Kobayashi, N.; Uesu, Y.; Hotta, C. Anomalous dielectric response in the dimer Mott insulator κ-(BEDT-TTF)$_2$Cu$_2$(CN)$_3$. *Phys. Rev. B* **2010**, *82*, 125119. [CrossRef]
37. Pinterić, M.; Čulo, M.; Milat, O.; Basletić, M.; Korin-Hamzić, B.; Tafra, E.; Hamzić, A.; Ivek, T.; Peterseim, T.; Miyagawa, K.; et al. Anisotropic charge dynamics in the quantum spin-liquid candidate κ-(BEDT-TTF)$_2$Cu$_2$(CN)$_3$. *Phys. Rev. B* **2014**, *90*, 195139. [CrossRef]

38. Rigaku Oxford Diffraction. *CrysAlis PRO*; Rigaku Oxford Diffraction: Yarnton, UK, 2015.
39. Petricek, V.; Dusek, M.; Palatinus, L. Crystallographic Computing System JANA2006: General features. *Z. Kristallogr.* **2014**, *229*, 345–352.
40. Hohenberg, P.; Kohn, W. Inhomogeneous Electron Gas. *Phys. Rev.* **1964**, *136*, B864. [CrossRef]
41. Kohn, W.; Sham, L.J. Self-Consistent Equations Including Exchange and Correlation Effects. *Phys. Rev.* **1965**, *140*, A1133. [CrossRef]
42. Soler, J.M.; Artacho, E.; Gale, J.D.; García, A.; Junquera, J.; Ordejón, P.; Sánchez-Portal, D. The SIESTA method for ab initio order-*N* materials simulation. *J. Phys. Condens. Matter.* **2002**, *14*, 2745–2779. [CrossRef]
43. SIESTA Code. Available online: http://departments.icmab.es/leem/siesta/ (accessed on 25 March 2018).
44. Artacho, E.; Anglada, E.; Diéguez, O.; Gale, J.D.; García, A.; Junquera, J.; Martin, R.M.; Ordejón, P.; Pruneda, J.M.; Sánchez-Portal, D.; et al. The SIESTA method; developments and applicability. *J. Phys. Condens. Matter* **2008**, *20*, 064208. [CrossRef] [PubMed]
45. Perdew, J.P.; Burke, K.; Ernzerhof, M. Generalized Gradient Approximation Made Simple. *Phys. Rev. Lett.* **1996**, *77*, 3865–3868. [CrossRef] [PubMed]
46. Troullier, N.; Martins, J.L. Efficient pseudopotentials for plane-wave calculations. *Phys. Rev. B* **1991**, *43*, 1993–2006. [CrossRef]
47. Kleinman, L.; Bylander, D.M. Efficacious Form for Model Pseudopotentials. *Phys. Rev. Lett.* **1982**, *48*, 1425. [CrossRef]
48. Artacho, E.; Sánchez-Portal, D.; Ordejón, P.; García, A.; Soler, J.M. Linear-scaling ab-initio calculations for large and complex systems. *Phys. Status Solidi (b)* **1999**, *215*, 809–817. [CrossRef]
49. Monkhorst, H.J.; Pack, J.D. Special points for Brillouin-zone integrations. *Phys. Rev. B* **1976**, *13*, 5188. [CrossRef]
50. Čulo, M.; Tafra, E.; Basletić, M.; Tomić, S.; Hamzić, A.; Korin-Hamzić, B.; Dressel, M.; Schlueter, J.A. Two-dimensional variable range hopping in the spin-liquid candidate κ-(BEDT-TTF)$_2$Cu$_2$(CN)$_3$. *Phys. B* **2015**, *460*, 208–210. [CrossRef]
51. The Crystallographic Data. Available online: https://www.ccdc.cam.ac.uk (accessed on 25 March 2018).
52. Guionneau, P.; Kepert, C.J.; Bravic, G.; Chasseau, D.; Truter, M.R.; Kurmoo, M.; Day, P. Determining the charge distribution in BEDT-TTF salts. *Synth. Met.* **1997**, *86*, 1973–1974. [CrossRef]
53. Novoa, J.J.; Whangbo, M.-H.; Williams, J.M. Ab Initio Computational Study of the C-H . . . Donor and C-H . . . Anion Contact Interactions in Organic Donor Salts. *Mol. Cryst. Liq. Cryst.* **1990**, *181*, 25–42. [CrossRef]
54. Whangbo, M.-H.; Jung, D.; Ren, J.; Evain, M.; Novoa, J.J.; Mota, F.; Alvarez, S.; Williams, J.M.; Beno, M.A.; Kini, A.M.; et al. *The Physics and Chemistry of Organic Superconductors*; Saito, G., Kagoshima, S., Eds.; Springer: Berlin/Heidelberg, Germany, 1990; pp. 262–266.
55. Aburto, A.; Orgaz, E. Ab initio electronic structure of the eclipsed and staggered conformations of the κ-(BEDT-TTF)$_2$Cu[N(CN)$_2$]Br organic superconductor. *Phys. Rev. B* **2008**, *78*, 113104. [CrossRef]
56. Pouget, J.P.; Alemany, P.; Canadell, E. Donor-Anion Interactions in Quarter-Filled Low-Dimensional Organic Conductors. In Preparation.
57. Pouget, J.-P.; Foury-Leylekian, P.; Alemany, P.; Canadell, E. Charge ordering in low dimensional organic conductors: Structural aspects. *Phys. Status Solidi (b)* **2012**, *249*, 937–942. [CrossRef]
58. Alemany, P.; Pouget, J.-P.; Canadell, E. Essential role of anions in the charge ordering transition of α-(BEDT-TTF)$_2$I$_3$. *Phys. Rev. B* **2012**, *85*, 195118. [CrossRef]
59. Dressel, M.; Lazić, P.; Pustogow, A.; Zhukova, E.; Gorshunov, B.; Schlueter, J.A.; Milat, O.; Gumhalter, B.; Tomić, S. Lattice vibrations of the charge-transfer salt κ-(BEDT-TTF)$_2$Cu$_2$(CN)$_3$: Comprehensive explanation of the electrodynamic response in a spin-liquid compound. *Phys. Rev. B* **2016**, *93*, 081201(R). [CrossRef]
60. Alemany, P.; Pouget, J.-P.; Canadell, E. Structural and electronic control of the metal to insulator transition and local orderings in the θ-(BEDT-TTF)2X organic conductors. *J. Phys. Condens. Matter* **2015**, *27*, 465702. [CrossRef] [PubMed]
61. Tomić, S.; Dressel, M. Ferroelectricity in molecular solids: A review of electrodynamic properties. *Rep. Prog. Phys.* **2015**, *78*, 096501. [CrossRef] [PubMed]
62. Itoh, K.; Itoh, H.; Naka, M.; Saito, S.; Hosako, I.; Yoneyama, N.; Ishihara, S.; Sasaki, T.; Iwai, S. Collective Excitation of an Electric Dipole on a Molecular Dimer in an Organic Dimer-Mott Insulator. *Phys. Rev. Lett.* **2013**, *110*, 106401. [CrossRef] [PubMed]

63. Fukuyama, H.; Kishine, J.-I.; Ogata, M. Energy Landscape of Charge Excitations in the Boundary Region between Dimer–Mott and Charge Ordered States in Molecular Solids. *J. Phys. Soc. Jpn.* **2017**, *86*, 123706. [CrossRef]
64. Foury-Leylekian, P.; Ilakovac, V.; Fertey, P. *Experimental Report n°: 20160753*; Cristal Beamline Experiment; Synchrotron Soleil: Saint-Aubin, France, 2017.
65. The 2c superstructure which develops below 200K in the Br salt should suppress the inter-donor inversion symmetry; See Nogami, Y.; Pouget, J.P.; Ito, H.; Ishiguro, T.; Saito, G. Superlattice structural transition in the organic superconductor χ-(BEDT-TTF)$_2$Cu [N(CN)$_2$]Br. *Solid State Commun.* **1994**, *89*, 113–116. [CrossRef]
66. The site symmetry breaking leads to a broad distribution of electronic density detected by ^{13}C NMR; De Soto, S.M.; Slichter, C.P.; Kini, A.M.; Wang, H.H.; Geiser, U.; Williams, J.M. ^{13}C NMR studies of the normal and superconducting states of the organic superconductor κ-(ET)$_2$Cu[N(CN)$_2$]Br. *Phys. Rev. B* **1995**, *52*, 10364–10368. [CrossRef]
67. Wzietek, P.; Mayaffre, H.; Jérome, D.; Brazovskii, S. NMR in the 2D Organic Superconductors. *J. Phys. I* **1996**, *6*, 2011–2041. [CrossRef]
68. Shimizu, A.; Hiramatsu, T.; Maesato, M.; Otsuka, A.; Yamochi, H.; Ono, A.; Itoh, M.; Yoshida, M.; Takigawa, M.; Yoshida, Y.; et al. Pressure-Tuned Exchange Coupling of a Quantum Spin Liquid in the Molecular Triangular Lattice κ-(ET)$_2$Ag$_2$(CN)$_3$. *Phys. Rev. Lett.* **2016**, *117*, 107203. [CrossRef] [PubMed]
69. Pinterić, M.; Lazić, P.; Pustogow, A.; Ivek, T.; Kuveždić, M.; Milat, O.; Gumhalter, B.; Basletić, M.; Čulo, M.; Korin-Hamzić, B.; et al. Anion effects on electronic structure and electrodynamic properties of the Mott insulator κ-(BEDT-TTF)$_2$Ag$_2$(CN)$_3$. *Phys. Rev. B* **2016**, *94*, 161105(R). [CrossRef]
70. Nakamura, Y.; Hiramatsu, T.; Yoshida, Y.; Saito, G.; Kishida, H. Optical Properties of a Quantum Spin Liquid Candidate Material, κ-(BEDT-TTF)$_2$Ag$_2$(CN)$_3$. *J. Phys. Soc. Jpn.* **2017**, *86*, 014710. [CrossRef]

© 2018 by the authors. Licensee MDPI, Basel, Switzerland. This article is an open access article distributed under the terms and conditions of the Creative Commons Attribution (CC BY) license (http://creativecommons.org/licenses/by/4.0/).